The intricate kinematics of the SB spiral galaxy NGC2613

Bottema, R

Published in:
Astronomy & astrophysics

Publication date:
1989

Astron. Astrophys. 225, 358–368 (1989)

ASTRONOMY
AND
ASTROPHYSICS

The intricate kinematics of the Sb spiral galaxy NGC 2613 ⋆

R. Bottema

Kapteyn Astronomical Institute, University of Groningen, P.O. Box 800, NL-9700 AV Groningen, The Netherlands

Received February 10, accepted June 29, 1989

Summary. In this paper the inclined ($i = 76°$) Sb spiral NGC 2613 is studied. Absorption line spectra are recorded along the major axis of the galaxy and radio observations in the 21 cm neutral hydrogen line are presented. The spectroscopic observations show that the stellar kinematics at some positions in the galaxy is quite intricate; irregular line profiles are observed. Although at first this seemed to be rather puzzling, a natural explanation followed when a galaxy model was employed. The ad hoc model consisted of two kinematical constituents: a bulge with constant velocity dispersion and prescribed rotation, together with a disk having a dispersion in the radial direction ($\langle v_R^2 \rangle^{1/2}$) decreasing exponentially with a scalelength twice the photometric scalelength and circular velocity inferred from the H I rotation curve. For the more regular East side a satisfactory fit to the data is found for $\langle v^2 \rangle^{1/2}_{\rm bulge} = 130\,{\rm km\,s^{-1}}$ and $\langle v_R^2 \rangle^{1/2}_{R=0} = 150 \pm 50\,{\rm km\,s^{-1}}$ for the disk. The rotation of the bulge is about half the disk rotation. For the West side the disk light drops more steeply which results in a region where bulge and disk are equally bright. If the same kinematical parameters as for the other side are used in that region, the same irregular profiles develop as the ones which are observed.

The H I observations were needed to determine the rotation curve which proved to be essentially flat at a level of $315\,{\rm km\,s^{-1}}$. The morphology of the gas distribution is (as the stellar kinematics) rather strange. Two gas blobs are rotating with the galaxy, positioned in opposite directions, well outside the stellar disk.

Key words: galaxies – kinematics and dynamics – structure – radio lines: 21 cm

1. Introduction

A project to study the stellar kinematics of late type spiral galaxies has been initiated by van der Kruit and Freeman (1984, 1986) and is continued by Bottema et al. (1987) and by Bottema (1988). In order to understand the stability and evolution of galactic disks knowledge about the stellar velocity dispersion is essential. The observational data obtained so far proved especially useful when compared with the predictions made by theoretical studies (Toomre, 1964; Binney and Lacey, 1988) and by n-body experiments (Ostriker and Peebles, 1973; Efstathiou et al., 1982; Sellwood and Carlberg, 1984).

In the course of the project a number of results have already been put forward. One of the most important conclusions is that the velocity dispersion of galactic disks decreases exponentially with radius, with a scalelength twice the photometric scalelength. This decrease in combination with the observed photometry and rotation gives a Q value which is about constant with radius as predicted by numerical experiments. Furthermore, the results for a number of galaxies indicate that the brighter galaxies have a larger velocity dispersion (Bottema, 1988).

In the paper presented here the study of random stellar motions is extended to the Sb spiral galaxy NGC 2613. This galaxy is rather massive and has a considerable bulge which complicates the analysis of the data substantially. Section 2 of this paper describes the spectroscopic observations and results. Due to the lack of emission lines NGC 2613 was also observed in the (radio) 21 cm hydrogen line of which the results and calculated rotation curve are presented in Sect. 3. Finally in Sect. 4 a kinematic galaxy model is constructed which is used for the interpretation of the kinematic data.

2. Spectroscopic observations

2.1. A description of the galaxy

NGC 2613 is a bright Sb spiral, classified by Sandage and Tammann (1981) as an Sb(s) (II) type. It has an angular extent of about $7' \times 2'$ on the sky and an inclination of 76°. In this paper a systemic velocity of $1665\,{\rm km\,s^{-1}}$ is derived which for a Hubble constant of $75\,{\rm km\,s^{-1}\,Mpc^{-1}}$ and correction for galactic rotation gives a distance of 19.3 Mpc. Table 1 gives a resumé of the most important physical parameters and Fig. 1 shows an optical photograph of the galaxy with the slit position (along the major axis) indicated.

2.2. Instrumental setup and observations

The spectroscopic observations of NGC 2613 were carried out from January 6 to 11, 1985 at the European Southern Observatory, La Silla in Chile. The 3.6 m telescope was used where at the Cassegrain focus the Boller & Chivens spectrograph was configured to produce a spectrum with a half power width resolution of about 1.5 Å, around 5100 Å (resolution $\sim 90\,{\rm km\,s^{-1}}$). The data were recorded on an RCA-CCD chip having a size of 512×320 pixels, 11 electrons per ADU, and a read-out noise of 3.5 ADU. The slit length of $3'$ covered the range of 153 pixels so the spatial length of 1 spectral row is $1''.18$. The

⋆ Based on observations collected at the European Southern Observatory, La Silla, Chile, and on observations collected with the Westerbork Synthesis Radio Telescope, The Netherlands.

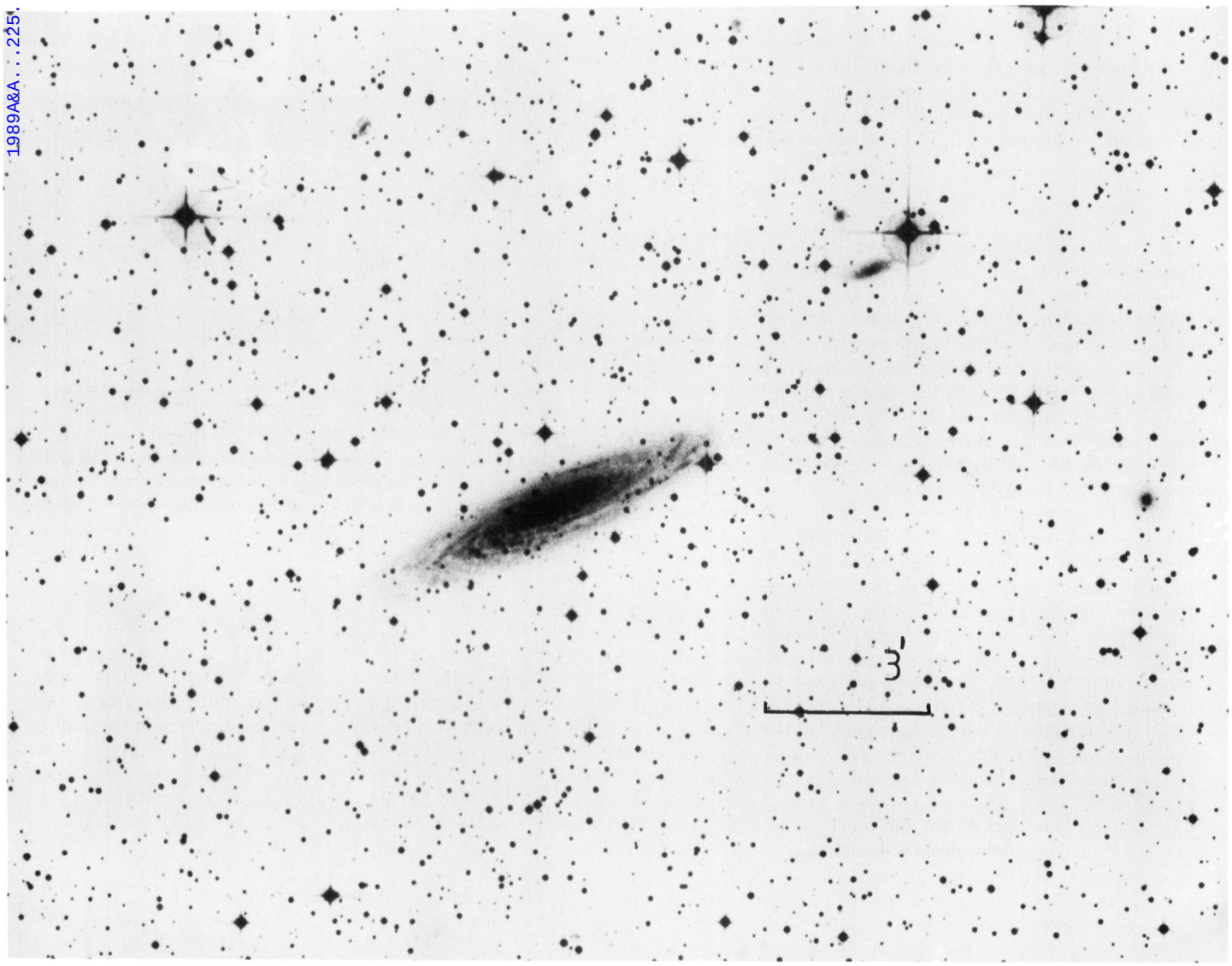

Fig. 1. A reproduction of the optical image of NGC 2613 from the ESO-SRC-J plate catalog. Spectroscopy is obtained along the whole major axis of the galaxy. North at top, East on left

Table 1. Physical parameters of NGC 2613

R.A. (1950)	$8^h31^m12^s$	This study
Declination (1950)	$-22°48'00''$	This study
H I syst. vel.	1665 km s^{-1}	This study
Max. rotational vel.	320 km s^{-1}	This study
Inclination	76°	Adopted
Pos. angle major axis	115°	Adopted
Distance	19.3 Mpc	Adopted
Hubble type	Sb(s) (II)	Shapley-Ames cat.
Int. blue mag. (B_T)	11.35	Shapley-Ames cat.

seeing during the observations ranged between two and three arcseconds and consequently always two to three spectral rows are correlated. Of the 512 pixels in the wavelength direction 500 were used ranging from 4842 to 5259 Å (417 Å) which after conversion to a velocity scale resulted in 49.55 km s^{-1} per pixel.

The slit was positioned along the major axis of the galaxy (Fig. 1). One end of the slit reached into the nightsky while the other end covered the central regions. In this way the South-East half of NGC 2613 was observed for 8^h30^m and the North-West side for 5^h51^m. Later on the two spectra of both sides were combined into one covering the whole major axis. The observations were divided up into single exposures of $1\frac{1}{2}$ to 2 h, each preceded by an exposure to a He-Ar calibration lamp. Several template stars were observed of spectral type close to K0III, also preceded by a calibration lamp exposure. At regular intervals zero second exposures were made to determine the bias level and readout noise. A long dark integration was made to check the dark current and flat field images were recorded by observing an illuminated white sheet attached to the dome.

Unfortunately, there were about 20 skylines in the spectrum that originated from infrared straylight of the first order spectrum of the same grating. Also the flat field exposures suffered infrared contamination. Hence these flat fields could certainly not be used to correct for the pixel-to-pixel response but still were useful to

largely correct for the large scale response of the chip. It turned out that the faint skylines could be properly subtracted but about five bright lines were so completely dominating the spectrum that at those wavelengths the spectrum could not be used. Before cross-correlation and after continuum subtraction these regions were set to zero and so did not enter in the cross-correlation sum.

2.3. *Data reduction*

The total data reduction proceeded along the standard lines, first from all the images the bias level was subtracted. The dark current amounted to less than 2 ADU's in one hour, so no correction was made for this. Next the cosmic rays were removed by comparing two spectral images, at the positions where the spectra differed substantially data were removed and replaced by the interpolated value of the surrounding pixels. The pollution by cosmic rays turned out to be approximately 1% of the chip for one hour integration. A correction for the large scale response of the chip was made by dividing the images by a normalized and strongly smoothed flat field exposure.

For the wavelength calibration ~ 12 lines were used spaced over the 417 Å interval, a second order polynomial was fitted in the wavelength direction and a third order in the slit direction. The standard deviation of the 12 lines from the wavelength solution was never larger than $5\,\mathrm{km\,s^{-1}}$. Then the exposures were re-gridded to a $\log\lambda$ scale with $49.55\,\mathrm{km\,s^{-1}}$ per pixel. Seperately for both sides of the galaxy all the exposures were added and subsequently the sky, determined by averaging a region at the end of the slit, was subtracted. In this way two spectral images, one of either side of NGC 2613 were constructed, for which in Fig. 2 the average number of ADU's as function of position along the slit is shown. The images of the East and West side were combined into one by shifting and adding, in this way a region of about 20″ around the nucleus has double counts. To all the spectral rows a polynomial was fitted to determine the continuum level. This level was subtracted, thus rejecting the line strength information but ensuring that at the faint levels where the continuum is ill defined the spectrum does not blow up by division through nearly zero.

The stellar spectra were bias subtracted, calibrated in wavelength, regridded to a $\log\lambda$ scale and then shifted to one common redshift. Two essentially noise free template spectra were constructed by twice averaging half of the stellar spectra. Like for the galaxy the continuum was removed by fitting a polynomial to the spectrum and subtracting this from the data.

Of the galaxy, spectra along the slit were averaged for a level >100 ADU's to determine the redshift and for levels >250 ADU's to determine the velocity dispersion. To this aim first the low frequency continuum and high frequency noise wavenumbers were filtered out. Regions heavily contaminated with skyline remnants were revalued to the average spectral value and then the cross-correlation was performed with the template spectra using Fourier techniques (Brault and White, 1971; Simkin, 1974; Tonry and Davis, 1979).

2.4. *Results of the spectroscopic observations*

The difference between the kinematical values resulting from the use of the two different template spectra was at most $2\,\mathrm{km\,s^{-1}}$. Compared with the intrinsic calibration error of about $5\,\mathrm{km\,s^{-1}}$ this difference is negligible. Hence only the results for the use of one template spectrum are presented. The cross-correlation functions from which the radial velocities are determined, are given as a contour plot in Fig. 3. As can be seen the cc peaks are quite irregular for a region on the West side of the galaxy, between 8″ and 20″ from the maximum intensity value. Over there the peaks are double or are having a plateau next to them. This cannot be explained by any instrumental effects and certainly not by any chip defects since in the middle of this region there is the transition from double counts where the sides are overlapping to single counts from the West side alone. The form of the cc peaks does not change when passing this transition. On the East side between 40″ and 50″ from maximum intensity the double peak effect is also

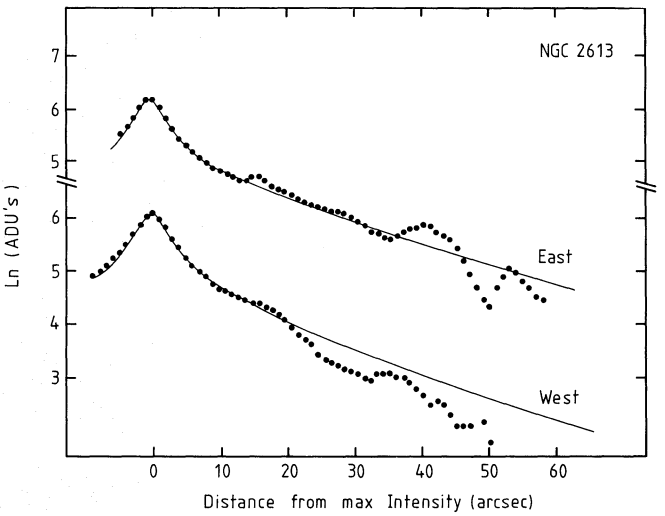

Fig. 2. The average number of counts (or Analog Digital Units for this CCD observation) over the wavelength range along the spectrograph slit. The lines represent the major axis photometry of a bulge-disk galaxy model used to explain the kinematics

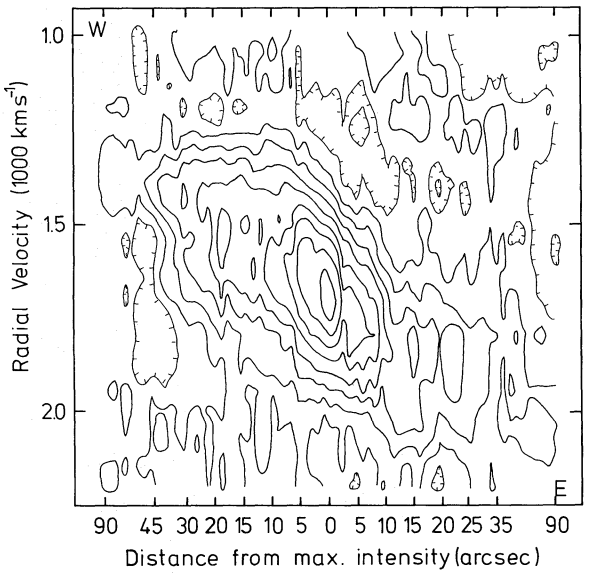

Fig. 3. The cross-correlation functions along the major axis of NGC 2613. The peak positions give the stellar radial velocities and the width is a measure for the velocity dispersions. Near the ends of the horizontal axis the scale is squeezed because spectra have been averaged along the slit until a countlevel of 100 ADU's. Contour levels are at equal intervals, the cross-hatched lines are negative. Because the continuum has been subtracted the contour values don't represent a physical quantity

Table 2. Stellar radial velocities

Distance from max. intensity (arcsec)	Helioc. radial vel. ($km\,s^{-1}$)	Distance from max. intensity (arcsec)	Helioc. radial vel. ($km\,s^{-1}$)
−96.2	1397	− 1.18	1658
−76.7	1342	0	1673
−71.4	1395	1.18	1684
−66.7	1368	2.36	1693
−62.0	1377	3.54	1707
−57.2	1365	4.72	1737
−53.1	1405	5.90	1740
−49.6	1371	7.08	1751
−46.0	1383	8.26	1750
−42.5	1405	9.44	1765
−38.9	1406	10.62	1756
−35.4	1433	11.80	1801
−32.5	1427	12.98	1829
−30.1	1430	14.16	1810
−27.73	1426	15.34	1790/1921
−25.37	1420	16.52	1816
−23.01	1435	17.70	1824
−21.24	1424	18.88	1830
−20.06	1434	20.06	1822
−18.88	1417/1601	21.24	1826
−17.7	1422/1604	22.42	1845
−16.52	1438/1580	23.60	1853
−15.34	1418/1612	25.37	1863
−14.16	1418/1607	27.73	1875
−12.98	1446/1616	30.09	1882
−11.8	1441/1626	32.45	1869
−10.62	1447/1607	34.81	1864
− 9.44	1618	37.17	1893
− 8.26	1438/1635	40.1	1910
− 7.08	1610	43.7	—
− 5.90	1634	47.2	1889
− 4.72	1612	51.3	1862
− 3.54	1625	56.1	1908
− 2.36	1639	89.7	1939

slightly present. In Bottema et al. (1987) it is shown that the cross-correlation function (ccf) is equal to the convolution of the stellar line profile with the autocorrelation function (acf) of the template spectrum

$$\begin{aligned} \mathrm{ccf} &= P * (S \star S) \\ &= P * \mathrm{acf}, \end{aligned} \tag{1}$$

where P is the line profile and S the instrumental profile. The acf is symmetric so the observed cc peak is a smoothed line profile which implies that the stellar line profile must have the same irregular form as the cc peak. Consequently it appears that between 8 and 20″ from the nucleus two stellar populations with different redshift are observed. These matters will be discussed extensively in Sect. 4.3. It should be remembered that the height of the cc peak is not a useful number since the continuum is subtracted; to check the reliability of the data one has to compare the peak with the noise in the region surrounding.

The stellar redshift is given be the peak position of the cc function, which was determined by fitting a 3, 5, and 7 point parabola to the peak and averaging the maxima. For the double peaked cc function both peak positions have been determined. The corresponding redshifts are given in Table 2 and shown graphically in Fig. 5. The determination of the stellar velocity dispersions proceeds in the same way as described in Bottema (1988), a grid of standard cross-correlation peaks is least squares fitted to the data. Table 3 gives the stellar velocity dispersions for all the spectra and Fig. 4 shows the fits to the observed cc functions. For the double peaks both peaks are fitted separately and as a whole. The errors were estimated by plotting the fits lying $30\,km\,s^{-1}$ from the best fitting value, it is obvious that for a double or otherwise irregular peak the error is large. All results below $40\,km\,s^{-1}$ are considered to be essentially unresolved and to range between 0 and $40\,km\,s^{-1}$. Finally in Fig. 6 the velocity dispersion is given as a function of distance from the position where the galaxy has its maximum intensity.

No emission could be detected in the spectra and hence no information was available about the kinematics of the gas. The absorption line spectra essentially give the kinematics of the old disk population. In order to model this stellar (old disk) kinematics knowledge of the young disk kinematics is essential. Thus NGC 2613 has been observed in the 21 cm neutral hydrogen line.

The effect of absorption on the observed velocity dispersions is expected to be very small. Generally galactic bulges do not contain any dust and consequently the dispersions observed in the bulge dominated region of NGC 2613 are not affected by absorption. For galactic disks the dominant region of absorption is the very thin layer of molecular clouds and dust where star formation takes place. No emission lines were detected in the spectrum of NGC 2613 which implies that there is very little star formation going on. This absence of young stars does not guarantee that there is no absorption at all, but does indicate that at least the density of molecular clouds and dust is small. Furthermore, the velocity dispersion of the old disk stars is being measured. The thickness of the old disk population is an order of magnitude larger than the thickness of a possible dust layer. So even if only the light from this side of the dust layer has been received the observed velocity dispersion is almost equal to the actual velocity dispersion of the locally isothermal old disk. Still, of course, a local absorption patch might cause a local deviation from the general velocity dispersion pattern, but inspection of the optical image of NGC 2613 shows that in the region where the spectroscopy yields results there are certainly no large absorption regions.

3. 21 cm line observations

3.1. The data

NGC 2613 was observed with the Westerbork Synthesis Radio Telescope for two five hour periods in January 1987. Because of the low declination of the source no full synthesis could be made. The digital line backend was configured for 64 frequency channels evenly spaced over a 5 MHz total bandwidth. After Hanning smoothing, this resulted in a velocity resolution equal to twice the channel spacing, or $33.3\,km\,s^{-1}$, FWHM. The frequency channels covered the velocity range from 1185 to $2250\,km\,s^{-1}$, while line emission was found over the range 1335 to $2052\,km\,s^{-1}$. The continuum was subtracted from the line channels by constructing a linear fit as a function of velocity to the encompassing line-free channels. From every channel the appropriate continuum was subtracted.

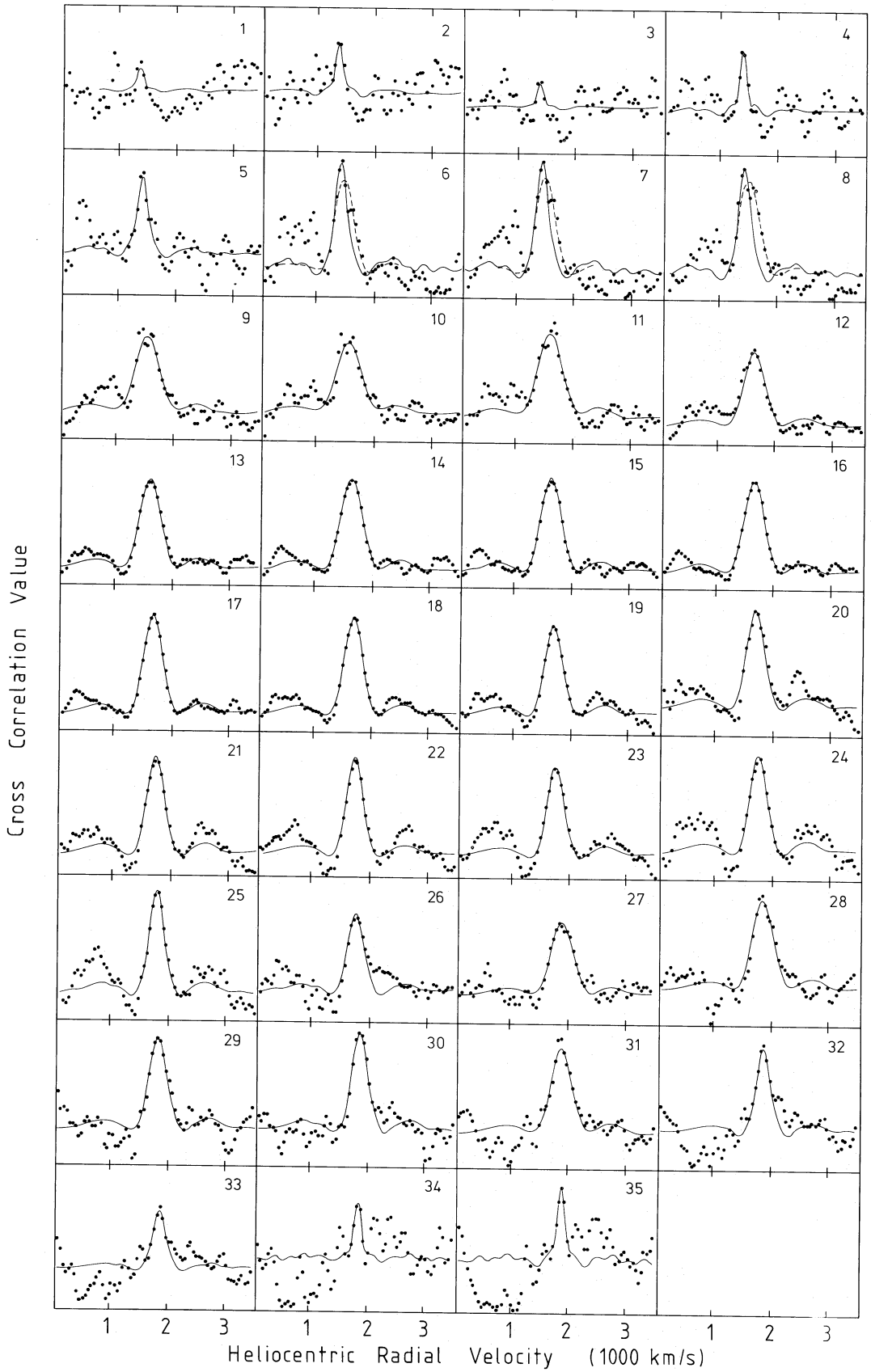

Fig. 4. All the cross-correlation peaks used to determine the stellar velocity dispersion. The drawn lines are the result of a least squares fit to the data. For some irregular peaks the fit is shown for the whole peak and the results for a fit forced over the narrow component alone. The numbers in the top right correspond to the numbers in Table 3. The signal-to-noise in panels 3 and 34 was judged to be so low that no reliable velocity dispersion could be determined

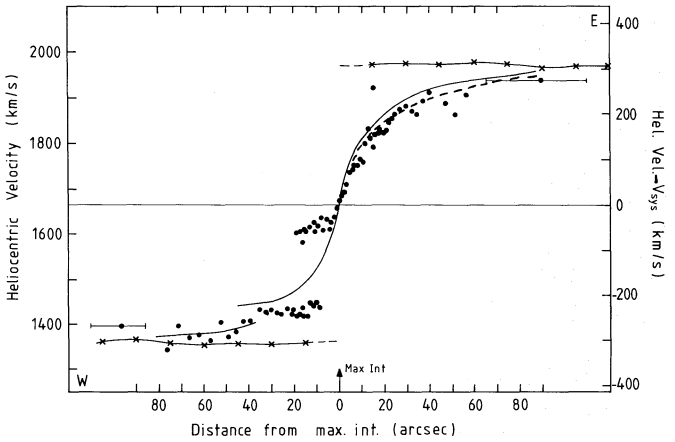

Fig. 5. The observed stellar radial velocities along the major axis (dots) and the H I rotation converted to radial velocities (crosses). The full drawn line represents the stellar radial velocities of the galaxy model with a central R-dispersion for the disk, $\langle v_R^2 \rangle_{R=0}^{1/2} = 150\,\mathrm{km\,s^{-1}}$ and bulge velocity dispersion of $130\,\mathrm{km\,s^{-1}}$. The dashed line is for $\langle v_R^2 \rangle_{R=0}^{1/2} = 200\,\mathrm{km\,s^{-1}}$

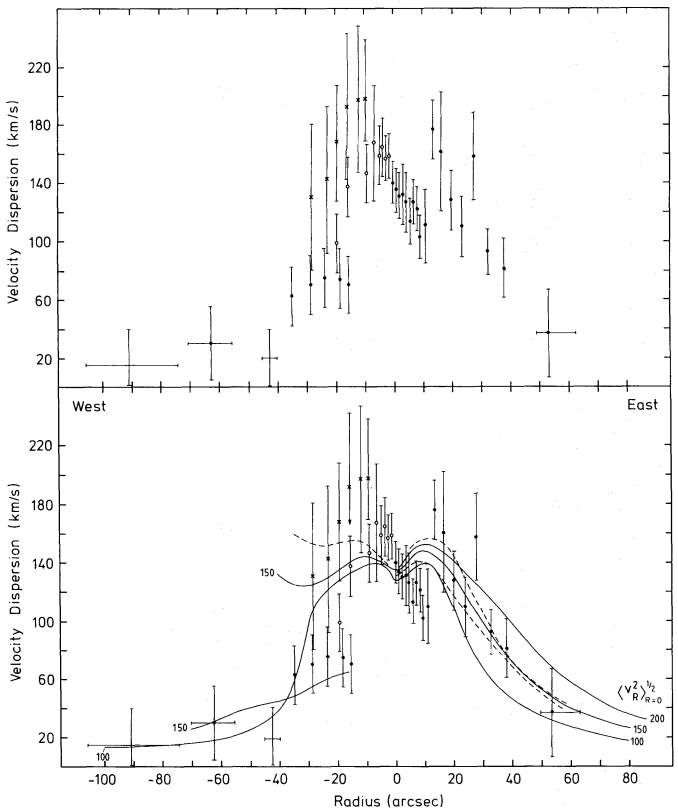

Fig. 6. *Top:* The observed stellar velocity dispersions along the major axis. For the region with irregular cross-correlation peaks the dispersion for the whole peak is given by the crosses and the dispersion for the narrow peak alone by the dots. The circles represent the dispersion for the broader component of the peak. *Bottom:* Resulting velocity dispersion for the model galaxy. The drawn lines are for a disk dispersion ($\langle v_R^2 \rangle_{R=0}^{1/2}$) of 100, 150, and 200 km s^{-1}, bulge dispersion of 130 km s^{-1} and bulge maximum rotation of 125 km s^{-1}. The upper dashed line is for a bulge rotation of 75 km s^{-1} and the lower dashed line for a bulge rotation of 200 km s^{-1}, keeping $\langle v_R^2 \rangle_{R=0}^{1/2}$ at 150 km s^{-1}

Table 3. Stellar velocity dispersions

No.	Distance from max. intensity (arcsec)	Velocity dispersion (km s^{-1})	Disp. error (km s^{-1})
1	−90.9	< 40	—
2	−62.5	30	25
3	−51.3	—	—
4	−42.5	< 40	—
5	−34.8	62	20
6tot	−28.3	130	50
6lv		70	20
7tot	−23.0	142	50
7lv		75	20
8tot	−18.9	167	40
8lv		74	20
8hv		98	20
9tot	−15.3	192	50
9lv		70	20
9hv		137	20
10	−11.8	197	50
11tot	− 8.9	198	40
11hv		146	20
12	− 6.5	167	40
13	− 4.7	158	20
14	− 3.5	164	20
15	− 2.4	156	15
16	− 1.2	158	15
17	0	139	15
18	1.2	134	15
19	2.4	130	15
20	3.5	131	20
21	4.7	126	20
22	5.9	113	15
23	7.1	126	15
24	8.3	121	15
25	9.4	102	15
26	11.2	110	25
27	13.6	176	20
28	16.5	160	40
29	20.1	127	20
30	23.6	109	20
31	27.7	157	30
32	32.5	92	15
33	37.8	81	20
34	44.3	—	—
35	53.1	37	30

tot: fit to total cc peak
lv: fit forced over low velocity component only
hv: fit forced over high velocity component only

The antenna pattern for this 2×5 h observation is complicated. Therefore the individual channel maps were "cleaned". Clean components were subtracted until the maximum residual was less than the rms noise level in the maps (1.4 K). The clean map was formed by convolving the point source clean components to a beam of 10″ × 64″ (HPBW, $\alpha \times \delta$) and adding this to the residual maps. These channel maps were smoothed to a beam of 30″ × 64″, which served as a mask to find the H I emission in the full resolution maps. For places where the intensity level was $> 3\sigma$ in

Table 4. H I rotational velocities

Radius (arcsec)	Rotational velocity ($km\,s^{-1}$)	Error ($km\,s^{-1}$)
0	—	–
15	315	4
30	318	3
45	315	3
60	323	4
75	317	4
90	307	3
105	313	4
120	315	14
135	317	16
150	320	20
165	313	20
180	314	15
195	312	15
210	310	9
225	306	4
240	297	3
255	290	5

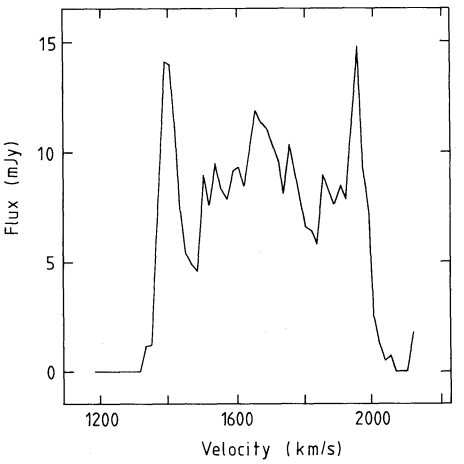

Fig. 7. The total H I profile of NGC 2613

the smoothed maps the data in the full resolution maps were retained ("conditional-transfer" method, Wevers et al., 1986).

Spatial integration of the channel maps formed in this way produced the H I spectrum (Fig. 7). Integration of this H I profile gives a flux density of $29.4\,Jy\,km\,s^{-1}$, which for a distance of 19.3 Mpc results in a total H I mass of $2.6\ 10^9\ M_\odot$. NGC 2613 has been observed with single dish telescopes by Reif et al. (1982), by Bottinelly et al. (1982) and by Fisher and Tully (1981), who find respectively a flux density of 125, 65 and $68\,Jy\,km\,s^{-1}$. The first paper shows a very noisy H I profile and the flux density value is very uncertain. The other papers agree on the amount of radiation. Because of the absence of the short spacing information the flux density of $\sim 30\,Jy\,km\,s^{-1}$ found here is in reasonable agreement with the value of the single dish observations.

To construct the total H I map the full resolution masked data were smoothed to a beam of $20'' \times 64''$ and added. The result is shown in Fig. 8, projected on an optical photograph of NGC 2613.

As for the stellar kinematics, the H I morphology is quite irregular and it seems that this galaxy simply refuses to cooperate with the observer. Most of the H I gas is confined to the stellar disk except for two distinct blobs, one on the North and one on the South side, situated at a distance from the centre of about twice the projected maximum stellar radius. The velocity field shows that these blobs follow the pattern of regular rotation given by the rest of the gas. Clearly observations with a better resolution are needed to explain the morphology in more detail. For this study the H I observations were only intended to determine the rotation curve. To this aim the kinematics is presented in a position velocity (or $l-v$) diagram, constructed by integration along lines perpendicular to the major axis of the galaxy. The total integration length was 6 arcmin, 3 on either side of the major axis so as to include most of the galaxy emission. The resulting diagram is in Fig. 9.

3.2. *Modelling of the* H I *rotation curve*

If spiral galaxies which are differentially rotating are observed with a large beam the observed H I kinematics will be severely affected by beam smearing. In one beam there is not only the gas rotating at the maximum rotational velocity but also gas away from the major axis, for which the full rotational velocity is not directed along the line of sight. Consequently the emission of the hydrogen is smeared to a velocity closer to the systemic velocity. This awkward beam smearing does, in this case, not allow a least squares fit of a tilted ring model to the velocity field as e.g. by Bosma (1978) or Begeman (1987), but instead a proper modelling of the H I is required.

To this aim the gas kinematics is simulated by means of a computer program. The galaxy was divided up into a number of concentric rings with a prescribed thickness, density, rotational velocity and velocity dispersion. The simulated emission was recorded in a data cube, just as for the observations. Then the cube was smoothed both spatially and in velocity to match the resolution of the observations and subsequently integrated perpendicular to the major axis to produce the $l-v$ diagram. All rings had the same inclination (76°), position angle (113°), thickness (325 pc, HPW) and velocity dispersion ($10\,km\,s^{-1}$). First the density was changed to resemble the intensities in the $l-v$ diagram, then the rotation was adapted and if this changes the intensities, the ring densities were changed again. In this way an iteration towards the observational data was performed, for both sides of the galaxy separately.

I shall now describe in detail the fitting of the rotation curve. First the dynamical centre has been determined at

R.A. (1950) = $8^h31^m12^s$
Dec. (1950) = $-22°48'00''$
Syst. velocity = $1665\,km\,s^{-1}$.

Then the velocities along the ridge lines (the velocity of the first maximum going, in velocity, from outside of the galaxy inwards to the systemic velocity) in the $l-v$ diagram were traced out. The values for the East and West side were averaged, corrected for inclination, and used as a first guess rotation curve (see Fig. 10). The modelling was done and the resulting position of the ridgeline compared with the data. It turned out that the input rotation had to be increased by about $20\,km\,s^{-1}$ after this first iteration. The model was run again and the input rotation corrected until the model matched the observations. Finally in the central regions the rotation curve lies about $25\,km\,s^{-1}$ above the rotation inferred from the ridgeline and in the outer parts about $15\,km\,s^{-1}$. In this

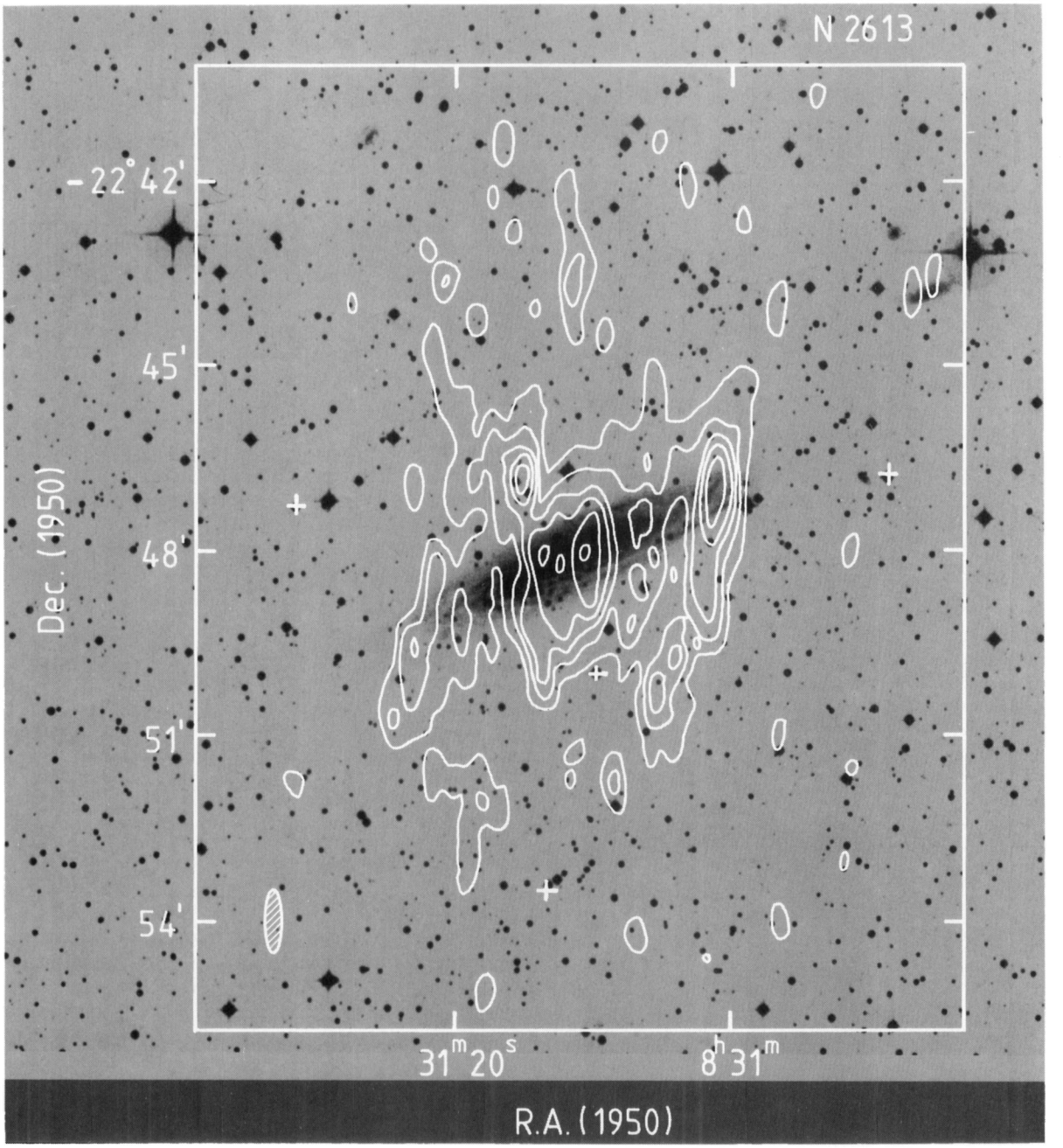

Fig. 8. The total H I map of NGC 2613 superposed on an optical photograph (*J*-band). The resolution amounted to $20 \times 64''$, ($\alpha \times \delta$, HPBW). Contours range from 1 to $6 \times 7.8\ 10^{19}$ H atoms cm^{-2} in steps of $7.8\ 10^{19}$ H atoms cm^{-2}. The two blobs of gas, one on the North and one on the South side take part in the regular rotation of the rest of the galaxy

way it proved possible to get an accuracy of a few km s^{-1} at those positions where the galaxy is symmetric. Between 120″ and 210″, however, the $l-v$ diagram is quite asymmetric and consequently the errors are larger. Between 120″ and 170″ the model ridge line cannot be determined for the East side and only a comparison with the West side is performed. The final rotational velocities are given in Table 4 and shown also in Fig. 10. It turns out that the rotation curve is nearly flat at a level of 315 km s^{-1}, which is quite typical for Sb spirals (Begeman, 1987). The model $l-v$ diagram resulting from this rotation is given in Fig. 9b and can be compared with the observation in Fig. 9a. The H I rotation was converted to radial velocities and projected on the model $l-v$ diagram (Fig. 9b) and is also compared with the stellar radial velocities in Fig. 5.

4. Stellar modelling

4.1. Description of the galaxy model

In order to understand the spectroscopic data, the galaxy needs to be properly modelled. By numerically integrating a kinematic model galaxy at those positions were it was observed line profiles

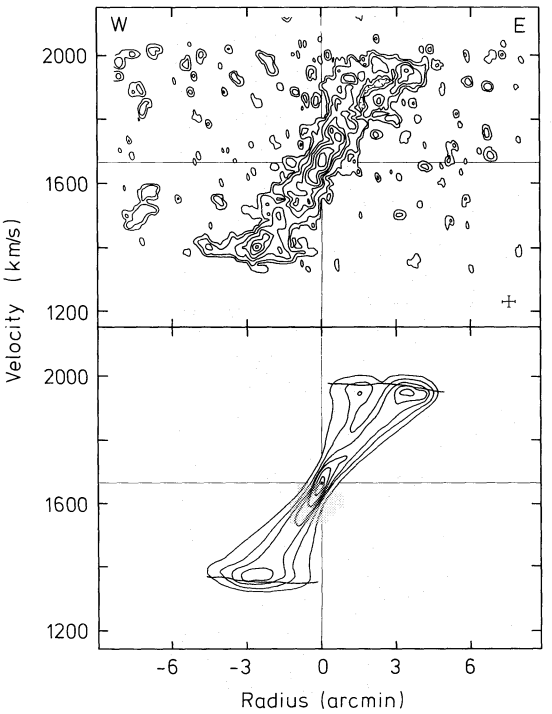

Fig. 9. *Top:* Position velocity map of the H I gas obtained by integration of the data cube perpendicular to the major axis over a length of 6′, 3′ on either side. Contour levels are at 1.3 K, 5.2 K to 67 K in steps of ~5.2 K. *Bottom:* The same position velocity map but not for a concentric ring model of the gas layer. The input rotation curve which is used, converted to radial velocities, is shown by the lines

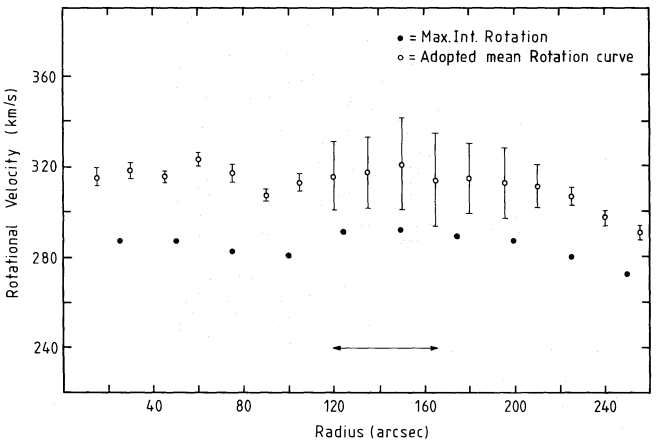

Fig. 10. Rotation implied by the ridge line of the $l-v$ diagram (dots). The open circles represent the final average rotation curve needed to put the ridge line at the indicated position. The double arrow indicates a region where for the South-East side of the galaxy the ridge line position is ill defined

will be constructed. A gaussian fit to these profiles gives a stellar velocity dispersion and radial velocity which can be compared with the observations. A complete discussion of this line profile fitting is given in Bottema et al. (1987) and will not be repeated here. Now first a description of the density structure will be given followed by an explanation of the kinematics.

The galactic disk was assumed to be locally isothermal, having constant thickness and M/L ratio

$$l^d = l_0^d\, e^{-R/h}\, \mathrm{sech}^2\left(\frac{z}{z_0}\right), \tag{2}$$

where l^d is the luminosity space density, h the photometric scalelength and z_0 indicating the thickness of the disk. A galaxy like NGC 2613 has a prominent bulge, which has to be included in the calculations. A similar Sb galaxy, NGC 891, has been studied by van der Kruit and Searle (1981), who show that the bulge component is flattened by the disk to a z/R ratio of about 0.5. For NGC 2613 this will be assumed also, together with luminosity density

$$l^b = l_0^b \left(1 + \left\{\frac{R^2}{R_c^2} + \frac{z^2}{\frac{1}{4}R_c^2}\right\}\right)^{-1}, \tag{3}$$

where l^b is the light space density of the bulge and R_c the core radius along the radial direction. Before including the disk and bulge density laws into the model the parameters h, R_c and l_0^b/l_0^d have to be determined from the photometry, the thickness z_0 was assumed to be fixed at 700 pc.

The disk kinematics is determined by the velocity dispersion and rotation as function of radius. For the velocity dispersion in the radial direction ($\langle v_R^2\rangle^{1/2}$) an exponential was assumed

$$\langle v_R^2\rangle^{1/2} \propto e^{-R/2h}, \tag{4}$$

with a scalelength twice the photometric scalelength as predicted for the dispersion in the z-direction for a locally isothermal selfgravitating disk. The velocity dispersion in the tangential direction is related to that in the radial direction by

$$\frac{\langle v_\theta^2\rangle}{\langle v_R^2\rangle} = \frac{B}{B-A}, \tag{5}$$

where A and B are the Oort constants. For a rotation curve which is almost flat as for NGC 2613 $\langle v_\theta^2\rangle \sim \frac{1}{2}\times\langle v_R^2\rangle$ at all radii. The velocity dispersion in the z-direction was assumed to have the same form as in Eq. (4) but is everywhere 0.6 times the value of the radial dispersion. For the inclination of NGC 2613 the kinematics in the z-direction hardly influence the observable motions. The input stellar rotation curve is given by the H I rotation diminished with the asymmetric drift of the stars (van der Kruit and Freeman, 1986; Binney and Tremaine, 1988). For a plane parallel disk this drift ($v_{\mathrm{rot}} - v_t$) is given by

$$v_{\mathrm{rot}}^2 - v_t^2 = \langle v_R^2\rangle\left[\frac{2R}{h} - \left(1 - \frac{B}{B-A}\right)\right], \tag{6}$$

which was assumed to give the actual stellar rotational velocity v_t.

For the bulge kinematics a simple model was assumed. The velocity dispersion is isotropic and constant like an isothermal sphere. The bulge is assumed to be cylindrically rotating with a rotation curve roughly consistent with the density distribution of Eq. (3)

$$v_{\mathrm{rot}}^b = v_{\mathrm{max}}^b \sqrt{1 - \frac{R_c}{R}\arctan\left(\frac{R}{R_c}\right)}. \tag{7}$$

I was led to this form of the bulge kinematics by observations of galactic bulges by Jarvis (1981), which show that both the velocity dispersion is almost constant with radius and the rotation resembles that of Eq. (7). The kinematic model is completely ad hoc and it therefore will be impossible to fit or explain all the details of the observations.

The disk and bulge model were included into one scheme. An inclination of 76° was given to the galaxy and the line profiles along the major axis were derived by numerical integration. First the density parameters were determined by comparing the model with the observations of the intensity along the slit.

4.2. *Fitting the slit intensity*

Before the spectroscopic data were analysed in detail an SRC-J plate of NGC 2613 was digitized and the photometric properties determined. This gave for an exponential fit to the disk a value for the scalelength of 41″.6 and central extrapolated face-on surface brightness of 19.32 J mag arcsec^{-2}. Unfortunately the photographic plate cannot be used for radii <1.5 arcmin because near the inner parts the photographic emulsion is saturated. And just at this inner region the spectroscopy gives results. Photometry given by a proper CCD image of the galaxy would be preferable but failing that there is still quite some information because the slit intensity gives the photometry along the major axis. At the fainter levels this intensity may be off considerably from the true photometric profile, but near the bulge the error will be very small.

The line profiles computed by the simulation program were simply integrated in velocity and the light density parameters h (scalelength of the disk), R_c (core radius) and I_0^b/I_0^d were iterated to a solution which fitted the slit intensity data the best. For the East side a disk scalelength of 25″ was found while for the West side this had to be smaller, 18″. The bulge parameters were $R_c = 2''.2 \pm 0''.2$ ($= 206 \pm 20$ pc) and $I_0^b/I_0^d = 22 \pm 1$. It should be noted that the disk scalelength near the inner regions is considerably smaller than that for the outer regions. An excellent photograph of NGC 2613 is found in "The Color Atlas of Galaxies" (Wray, 1988). It shows that indeed the bulge is not in the centre of the galaxy, being displaced to the West. Finally it should be noted that this bulge-disk decomposition is very preliminary but that nevertheless it will give a good handle on how bulge and disk influence the kinematics.

4.3. *Fitting the stellar kinematics*

The bulge and disk density parameters were put into the simulation and line profiles calculated for both the East and West side separately. First I shall discuss the results for the East side. Figure 6 shows the fits for a model with a bulge dispersion of 130 km s^{-1} and maximum rotation of 125 km s^{-1}. The disk had a central R-dispersion $\langle v_R^2 \rangle_{R=0}^{1/2}$ of 100, 150, and 200 km s^{-1}. Although the data between 5 and 10″ cannot be fitted very well, on the whole the fit is quite satisfactory. In general the model line profiles are rather symmetric, also in the bulge-disk transition region. The bulge rotation cannot really be determined from the kinematic data presented here. A smaller bulge rotation causes a stronger increase in dispersion going from the centre outwards because the line profiles are becoming broader. Therefore also the dispersions for $v_{\max}^{\text{bulge}} = 75$ and 200 km s^{-1} together with a central disk dispersion of 150 km s^{-1} are given by the dashed lines. On the bases of the modelling of the data for the East side it can be concluded that $\langle v_R^2 \rangle_{R=0}^{1/2} = 150 \pm 50$ km s^{-1} for the disk.

Modelling of the West side of NGC 2613 gave some unexpected results. Here the scalelength of the disk is smaller than for the other side which has as consequence that the disk light is more steeply dropping with radius. The intensity of the bulge and disk turn out to be about equal over a range of radii producing rather asymmetric line profiles. On the high velocity side there is the narrow disk profile and going to lower rotational velocities a broad plateau is attached to it originating from the bulge having a large velocity dispersion. At these transition radii there are the observed irregular or double cross-correlation peaks which signifies a more distinct two component structure than the modelling gives. The model is just ad hoc and in reality there can be locally a different light intensity for the components or a different kinematics. The fact that at the same places in the observations and in the model the line profiles are complex does however clearly indicate that the almost equality in intensity and different kinematics of disk and bulge is the cause of this irregularity.

The standard procedure to determine velocity dispersion and radial velocity by fitting a gaussian to the line profile can probably not be followed at some radii. An automatic fit causes a jump in position of the gauss fit near $R = 30''$. In Fig. 6 the velocity dispersion as a function of radius is indicated for $\langle v_R^2 \rangle_{R=0}^{1/2} = 100$ and 150 km s^{-1}. Between 20 and 40″ for the 150 km s^{-1} case an automatic fit to the total line profile is shown and also a fit forced over the narrow component alone. This last fit is rather uncertain because it depends somewhat on the velocity range to which the fit is made, but still the data and model seem to agree quite good. If the disk is given a central dispersion of 100 km s^{-1} the change in line profiles with radius behaves more smoothly. As for the East side the bulge rotation is also a parameter which cannot be properly determined. Lowering the bulge rotation, again gives an increased velocity dispersion at radii until 40″. Because the bulge light is everywhere so dominant compared to the disk the kinematics of the two come out so very intertwined that a proper determination of the disk velocity dispersion cannot be performed. The only conclusion that can be made is that a central dispersion in the radial direction of ~ 150 km s^{-1} (as for the East side) is not in conflict with the observations.

Also the radial velocities produced by the model can be compared with the data. In Fig. 5 the result for $\langle v_R^2 \rangle^{1/2} = 150$ and 200 km s^{-1} are shown projected on the observations. For the more regular East side a central R-dispersion of 200 km s^{-1} is favoured. Unfortunately however, the calculation and results of the stellar radial velocities should be considered with some scepsis because integration effects play a major role. Certainly for the inner 40″ the shape of the line profiles is much more dependent on the dispersions and actual shape of bulge and disk than on the stellar rotation. Thus, although a central R-dispersion of 200 km s^{-1} fits the observed data better, a dispersion of 150 km s^{-1} can certainly not be ruled out. On the West side as already mentioned before the irregular profile region cannot be reproduced completely. Instead the fit to the asymmetric model profiles gives an intermediate velocity together with a jump around $R = 35''$. Beyond 40″ where essentially only the disk radial velocities are measured the fit for $\langle v_R^2 \rangle_{R=0}^{1/2} = 150$ km s^{-1} is very satisfactory.

In general it should be remembered that for an Sb type galaxy like NGC 2613 with a considerable inclination the observed stellar "radial velocities" say very little about the actual stellar rotation of disk and bulge. Hence it is useless to attempt for instance a construction of a mass model for such a galaxy based on absorption line measurements alone.

4.4. *Discussion*

An Sb galaxy like NGC 2613 with a prominent bulge shows an intricate stellar kinematics. To study galactic disks, it is of course easier to observe pure disk systems and for bulges, bulge-dominated galaxies. Unfortunately, Sb and Sa galaxies which are generally intrinsically brighter than Sc systems always (per

definition) have a large bulge. Despite the complexity of the galaxy studied here a few conclusions can be drawn.

First the bulge and disk are two separate kinematic systems. The bulge is certainly rotating much slower than the disk at equal radii and probably has a constant velocity dispersion around 130 km s^{-1}. Mainly based on the modelling of the data for the East side an exponentially decreasing velocity dispersion in the radial direction with a scalelength twice the photometric scalelength fits the observations very satisfactorily for $\langle v_R^2 \rangle_{R=0}^{1/2} = 150 \pm 50$ km s^{-1}. This value is, for a system with the dimensions of NGC 2613 ($v_{max} \sim 315$ km s^{-1}), rather low compared to for example the results of NGC 7184 (van der Kruit and Freeman, 1986), a central dispersion around 200 km s^{-1} would have been more in the line of expectation. Another clear finding is that for the inner radii the final stellar radial velocities are mainly determined by integration effects. Care should be taken when interpreting such observations for other Sb like systems.

A calculation of Toomre's Q-parameter (Toomre, 1964) is, considering the large uncertainties in photometry and kinematics, not very useful. Spectra of the galaxy NGC 7331 which is an almost look-alike of NGC 2613 have been obtained now and detailed photometry of this galaxy is available (Kent, 1987). In the near future the results will be presented which may hopefully shed some more light on a possible distinct kinematical structure of bulges and disks of spiral galaxies.

Acknowledgements. The author wishes to thank the staff of the Netherlands Foundation for Radio Astronomy for letting me use their computer facilities in order to reduce the spectroscopic data. I also thank A. Pickles for introducing me to the software package Pandora and P. van der Kruit for valuable advise and encouragement during the course of this project.

References

Begeman, K.: 1987, Ph. D. Thesis, Groningen State University
Binney, J., Lacey, C.: 1988, *Monthly Notices Roy. Astron. Soc.* **230**, 597
Binney, J., Tremaine, S.: 1987, *Galactic Dynamics*, Princeton University Press, Princeton, NJ
Bosma, A.: 1978, Ph. D. Thesis, Groningen State University
Bottema, R.: 1988, *Astron. Astrophys.* **197**, 105
Bottema, R., Kruit, P.C. van der, Freeman, K.C.: 1987, *Astron. Astrophys.* **178**, 77
Bottinelly, L., Gouguenheim, L., Paturel, G.: 1982, *Astron. Astrophys.* **113**, 61
Brault, J.W., White, O.R.: 1971, *Astron. Astrophys.* **13**, 169
Efstathiou, G., Lake, G., Negroponte, J.: 1982, *Monthly Notices Roy. Astron. Soc.* **199**, 1069
Fisher, J.R., Tully, R.B.: 1981, *Astrophys. J. Suppl.* **47**, 139
Jarvis, B.J.: 1981, Ph. D. Thesis, Australian National University
Kent, S.M.: 1987, *Astron. J.* **93**, 816
Kruit, P.C. van der, Freeman, K.C.: 1984, *Astrophys. J.* **278**, 81
Kruit, P.C. van der, Freeman, K.C.: 1986, *Astrophys. J.* **303**, 556
Kruit, P.C. van der, Searle, L.: 1981, *Astron. Astrophys.* **95**, 116
Ostriker, J.P., Peebles, P.J.E.: 1973, *Astrophys. J.* **186**, 467
Reif, K., Mebold, U., Goss, W.M., Woerden, H. van, Siegman, B.: 1982, *Astron. Astrophys. Suppl.* **50**, 451
Sandage, A., Tammann, G.A.: 1981, *A revised Shapley-Ames Catalog of Bright Galaxies*, Carnegie Institute of Washington
Sellwood, J.A., Carlberg, R.G.: 1984, *Astrophys. J.* **282**, 61
Simkin, S.M.: 1974, *Astron. Astrophys.* **31**, 129
Tonry, J., Davis, M.: 1979, *Astron. J.* **84**, 1511
Toomre, A.: 1964, *Astrophys. J.* **139**, 1217
Wevers, B.M.H.R., Kruit, P.C. van der, Allen, R.J.: 1986, *Astron. Astrophys. Suppl.* **66**, 505
Wray, J.D.: 1988, *The Color Atlas of Galaxies*, Cambridge University Press, Cambridge